Journal of ELECTRONIC MATERIALS, Vol. 48, No. 9, 2019
https://doi.org/10.1007/s11664-019-07315-2

High Thermoelectric Properties in $Mg_2Ge_{0.25}Sn_{0.75-x}Sb_x$ Solid Solution

WEIQIN AO,[1,2,3] MIAO PENG,[2] FUSHENG LIU,[2] JUNQIN LI,[2] YONG DU,[1] SHUHONG LIU,[1] and CHENGYING SHI[1]

1.—State Key Laboratory of Powder Metallurgy, Central South University, Changsha 410083, China. 2.—College of Materials Science and Engineering, Shenzhen University, Guangdong Research Center for Interfacial Engineering of Functional Materials and Shenzhen Key Laboratory of Special Functional Materials, Shenzhen 518060, China. 3.—e-mail: aomily@126.com

Mg_2Sn-based solid solutions $Mg_2Ge_{0.25}Sn_{0.75-x}Sb_x$ (x = 0, 0.03, 0.05, 0.07, 0.10, 0.15) were synthesized by high-frequency melting in a graphite crucible, followed by spark plasma sintering. The effects of Sb substitution on the phase constitution and thermoelectric properties of the solution were investigated. All the samples were face-centered cubic $Mg_2Ge_{0.25}Sn_{0.75}$ solutions without any additional phase arising from Sb in the compounds. The electrical resistivity decreased significantly from 202 $\mu\Omega$ m to 3.66 $\mu\Omega$ m at 300 K as lower Sb content x increased from 0 to 0.03, but increased slightly from 3.66 $\mu\Omega$ m to 11.6 $\mu\Omega$ m at 300 K as Sb content x further increased from 0.03 to 0.15. The Seebeck coefficient showed a similar pattern of change. The thermal conductivity of the solid solution clearly decreased from 3.6 W m^{-1} K^{-1} to 1.4 W m^{-1} K^{-1} at 300 K as Sb content x increased from 0 to 0.15. The highest power factor of 4010 μW m^{-1} K^{-2} was obtained in the sample of $Mg_2Ge_{0.25}Sn_{0.72}Sb_{0.03}$ at 573 K. The lowest thermal conductivity of 1.17 W m^{-1} K^{-1} was found in $Mg_2Ge_{0.25}Sn_{0.65}Sb_{0.1}$ at 473 K. The maximum ZT of 1.54 was obtained in $Mg_2Ge_{0.25}Sn_{0.68}Sb_{0.07}$ at 623 K. Compared with the value 0.03 for its parent alloy at the same temperature, this is a dramatic improvement.

Key words: Thermoelectric material, Mg_2Sn-based alloys, Sb-dopant, high thermoelectric properties

INTRODUCTION

Thermoelectric (TE) materials can directly convert waste heat (such as car and plane exhaust heat) into electricity by utilizing the Seebeck effect, without consuming any other energy. The properties of thermoelectric materials can be evaluated with a dimensionless figure of merit (ZT), defined as $ZT = \frac{S^2T}{\rho k}$, where S, ρ, T and k are the Seebeck coefficient, electrical resistivity, absolute temperature and thermal conductivity, respectively. The above equation indicates that a good TE material requires a high Seebeck coefficient and low electrical resistivity, but at the same time requires low thermal conductivity.[1] However, the ZT values of materials used commercially are around 0.8, which corresponds to about 10% Carnot efficiency. Therefore, many researchers around the world are making great efforts to improve the ZT value of TE materials. Although significant enhancement of ZT values has been reported in superlattices,[2,3] it is generally difficult to use these superlattices in large-scale energy-conversion applications because of both heat transfer and cost limitations.[4]

The magnesium compounds Mg_2X (X = Si, Ge, Sn) and their solid solutions have attracted increasing attention as promising thermoelectric materials at temperatures from 500 K to 800 K, as they are non-toxic, environmentally friendly and abundantly

(Received April 22, 2018; accepted May 21, 2019; published online June 17, 2019)

available.[5–11] Mg_2X compounds with an anti-fluorite structure are narrow-band-gap semiconductors with indirect band gaps of 0.77 eV, 0.74 eV and 0.35 eV, respectively.[12] The material factor $\beta = (m^*/m_e)^3/2\mu\kappa_l^{-1}$ can be utilized as the criterion for thermoelectric material selection, where m^* is the density-of-state effective mass, m_e is the mass of an electron, μ is carrier mobility and κ_l is thermal conductivity.[12] That is to say, TE materials with high ZT values should have relatively high β values, low lattice thermal conductivity and high carrier mobility. According to the literature, the β for magnesium compounds Mg_2X is 3.7–14, which is higher than the values for silicon–germanium alloys with 1.2–2.6.[13,14] Extensive research efforts have recently been devoted to Mg_2X compounds because of their potential thermoelectric properties.

The thermal conductivity of pure Mg_2X (X = Si, Ge, Sn) at room temperature is above 6 W m^{-1} K^{-1}, and this high thermal conductivity results in a relatively low dimensionless thermoelectric figure of merit.[15] To improve the thermoelectric figure of merit of Mg_2X (X = Si, Ge, Sn) compounds, tremendous effort has been invested in research into Mg_2Si-Mg_2Sn and Mg_2Si-Mg_2Ge solid solutions, which are expected to have an optimized band structure and reduced phonon thermal conductivity. For Mg_2Si-Mg_2Sn, Liu et al. found that for the $Mg_2Si_{0.3}Sn_{0.7}$ solid solution, thermal conductivity was further reduced to about 2.1 W m^{-1} K^{-1} at T = 623 K, and the maximum ZT value reached 1.3 for the two solid solutions.[16] Investigations by Zhang et al.[17] revealed that Sb doping strongly increased the density of point defects and enhanced lattice distortion in $Mg_2(Si_{0.4-x}Sb_xSn_{0.6})$ samples, which reduced lattice thermal conductivity due to the increased scattering of phonons. Al-doped $Mg_2Si_{0.4}Sn_{0.6}$ was found to increase the Seebeck coefficient and reduce the thermal conductivity, and achieved the highest dimensionless figure of merit ZT = 1.30 at 773 K compared with the highest ZT value of 0.12 for $Mg_2Si_{0.4}Sn_{0.6}$ at 550 K.[18] For Mg_2Si-Mg_2Ge alloys, Sb and Bi doping reduced the thermal conductivity more at temperatures above 723 K due to ionized impurity scattering and significantly improved the ZT. The highest ZT value of 0.56 for $Mg_2Si_{0.5}Ge_{0.5}Sb_{0.02}$ and 0.79 for $Mg_2Si_{0.7}Ge_{0.3}Bi_{0.02}$ was higher than 0.05 for $Mg_2Si_{0.5}Ge_{0.5}$ at 823 K.[12,19]

However, there is scant literature concerning the thermoelectric properties of Mg_2Sn-Mg_2Ge compounds. According to Mg_2Ge and Mg_2Sn pseudo-binary phase diagrams, a solid solution of $Mg_2Ge_xSn_{1-x}$ exists in the range of x content between 0 and 0.4.[20] Solid solutions of Mg_2Sn and Mg_2Ge can reduce thermal conductivity and increase the Seebeck coefficient due to enhanced phonon scattering by substitution of Ge for Sn. Therefore, we prepared samples of $Mg_2Ge_xSn_{1-x}$ with x = 0.15 to 0.3 to obtain solid solutions and to investigate their thermoelectric properties. Earlier work in this system was reported by Liu et al.[21] It was found that $Mg_2Sn_{0.75}Ge_{0.25}$ has an average ZT of 0.9 and PF of 52 μW cm^{-1} K^{-2} over a temperature range of 25–450°C, a peak ZT of 1.4 at 450°C, and peak PF of 55 μW cm^{-1} K^{-2} at 350°C.[21] Many recent studies[17,19] have shown Sb and Bi to be promising dopants in the Mg_2(Sn,Si) system by enhancing ZT, but research on Sb dopants in Mg_2Sn-Mg_2Ge is rarely reported. In this work we selected $Mg_2Ge_{0.25}Sn_{0.75}$ as the parent alloy in order to explore a new way to prepare Mg_2Sn-Mg_2Ge-based solid solutions and to improve the thermoelectric properties through Sb substitution for Sn atoms. The alloys were prepared by high-frequency melting and spark plasma sintering (SPS) in a very short time, which has not been reported before. The SPS technique is known for its high efficiency in densification of materials at relatively low temperature under compression, using pulsed DC current through punches and graphite die. The pulsed DC current promotes fast heating of the powder by charging the intervals between powder particles with electrical energy and effectively applying a high-temperature spark plasma. It is one of the most innovative and promising methods for powder sintering, as evidenced by the maximum ZT of 1.54 obtained in this work, much higher than the peak value of 1.4 reported previously.[21]

EXPERIMENT DETAILS

The elements Mg, Ge, Sn and Sb with 99.99% purity were used as starting materials. They were mixed in the appropriate molar ratio of the $Mg_2Ge_xSn_{1-x}$ alloys, and the $Mg_2Ge_xSn_{1-x}$ alloys with x = 0.15, 0.20, 0.25, 0.30 were prepared to confirm the solid solution range. Then the $Mg_2Ge_{0.25}Sn_{0.75}$ solid solution was selected as the parent alloy and the $Mg_2Ge_{0.25}Sn_{0.75-x}Sb_x$ alloys with x = 0, 0.03, 0.05, 0.07, 0.10, 0.15 were prepared and investigated. To compensate for Mg evaporative loss, Mg was added in excess of 10 wt.%. The mixtures were packed in graphite crucibles and placed in quartz tubes. After evacuation under a vacuum at 3×10^{-3} Pa and filling with 0.05 MPa argon, the raw materials in the quartz tube were melted for 1 min by high-frequency melting at a current of 250 A and frequency of 100 kHz. The filling of tubes with 0.05 MPa argon before high-frequency melting was to ensure that the Mg and the graphite crucible were isolated from O and that the volatilization of Mg was effectively reduced. Also, the high-frequency melting method has the advantage of shortening the reaction time considerably. After 30 h annealing in a furnace, the samples were milled into powders, then put in a graphite cylinder die and sintered at a temperature of 953 K and pressure of 50 MPa for 5 min by spark plasma sintering (SPS). Next, 15-mm disks were cut to dimensions of 13 mm × 5 mm × 5 mm for the measurement of electrical properties and

Φ10 mm × 2 mm for the thermal conductivity measurement.

The phases in all samples were analyzed by x-ray diffraction using a Bruker D8 Advance SS/18 kW diffractometer with CuK_α radiation, TOPAS software and Jade5 software. The Seebeck coefficient (S) and electrical resistivity (ρ) were measured by an ULVAC-RIKO ZEM-2 apparatus (Japan) in a helium atmosphere, and thermal conductivity (κ) was measured by a laser flash thermal constant measuring system (TC-9000H, ULVAC-RIKO, Japan). The bulk density of the sample was calculated from the sample geometry and mass. The Hall coefficient at room temperature was measured using the van der Pauw technique under a reversible magnetic field of ± 5 T on a QuantumDesign Physical Property Measurement System PPMS-9. The microstructure was observed by scanning electron microscopy (SEM) with energy-dispersive x-ray spectroscopy (EDS) (SU-70, Hitachi).

RESULTS AND DISCUSSION

Phase Analysis

Figure 1 shows the x-ray diffraction patterns for the samples of $Mg_2Ge_xSn_{1-x}$ and Sb-doped $Mg_2Ge_{0.25}Sn_{0.75}$ compounds. The pattern of the solid solutions is a face-centered cubic (fcc) phase and corresponds to Mg_2Sn (ICDD PDF #07-0274) and Mg_2Ge (ICDD PDF #02-1135), with all the peaks located between pure Mg_2Sn and Mg_2Ge. From Fig. 1a we can see that $Mg_2Ge_xSn_{1-x}$ solid solutions were successfully prepared with x from 0.15 to 0.3. Only the cubic phase was observed and no secondary phase was found. Their diffraction peaks gradually shifted to higher angles with increasing Ge content. The lattice parameters of $Mg_2Ge_xSn_{1-x}$ solid solutions were calculated using the Rietveld refinement method with TOPAS software, and are presented in the inset in Fig. 1a. Here, we can see that the lattice constant decreased linearly from 6.707 Å to 6.649 Å with increasing Ge content from 0.15 to 0.3, between the values of Mg_2Ge (6.394 Å) and Mg_2Sn (6.763 Å), respectively, which was in agreement with the peak shifts and obeyed Vegard's law.

Figure 1b shows that pure $Mg_2Ge_xSn_{1-x}$ solid solutions were obtained and all the doped Sb atoms were dissolved in the fcc $Mg_2Ge_{0.25}Sn_{0.75}$ solutions without any additional phase arising from Sb in the compounds. The diffraction peaks shifted to higher 2θ angle with the increase in Sb due to the substitution of smaller Sb for Sn atoms in the compounds. The inset in Fig. 1b presents the lattice constant variations of the Sb-doped $Mg_2Ge_xSn_{1-x}$ compounds. The lattice constants of $Mg_2Ge_{0.25}Sn_{0.75-x}Sb_x$ decreased gradually from 6.689 Å to 6.672 Å with increasing Sb content. The decrease was small because the doping concentration was very low. Therefore, the data in Fig. 1 obey Vegard's law,[22] indicating that the $Mg_2Ge_xSn_{1-x}$

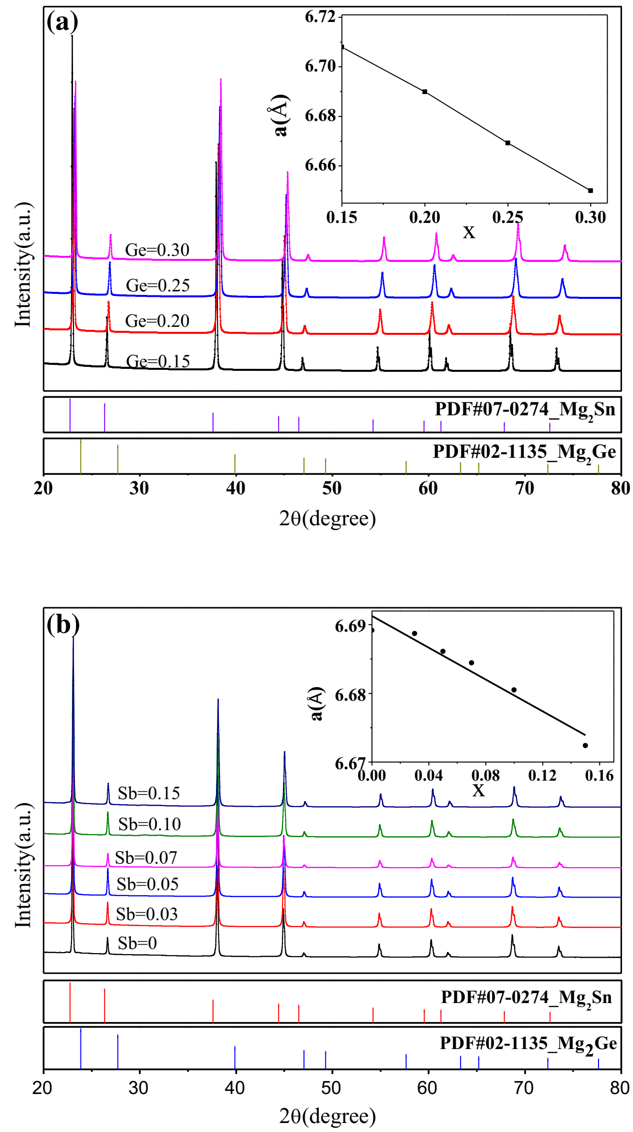

Fig. 1. X-ray diffraction patterns for the samples of (a) $Mg_2Ge_xSn_{1-x}$ (x = 0.15, 0.20, 0.25 and 0.30) and (b) $Mg_2Ge_{0.25}Sn_{0.75-x}Sb_x$ (x = 0, 0.03, 0.05, 0.07, 0.10 and 0.15). Insets in the figures show the lattice parameters of $Mg_2Ge_xSn_{1-x}$ and $Mg_2Ge_{0.25}Sn_{0.75-x}Sb_x$ solid solutions, respectively.

and $Mg_2Ge_{0.25}Sn_{0.75-x}Sb_x$ solid solutions were well formed. The distortions caused by the substitution of the Sb atoms for the Sn atoms in these single phases may affect the electrical and thermal transport and thus enhance the thermoelectric performance.

The microstructure and composition of the phases in the alloys were observed and analyzed by scanning electron microscopy (SEM) with EDS. Typical SEM images and EDS results for representative samples of $Mg_2Ge_{0.25}Sn_{0.75-x}Sb_x$ with x = 0 and 0.07 after SPS are shown in Fig. 2. Figure 2b and d shows the EDS results for the samples in Fig. 2a and c, respectively. The SEM images in Fig. 2a and c reveal that the $Mg_2Ge_{0.25}Sn_{0.75-x}Sb_x$ alloys formed a single phase with solid solution, and no secondary

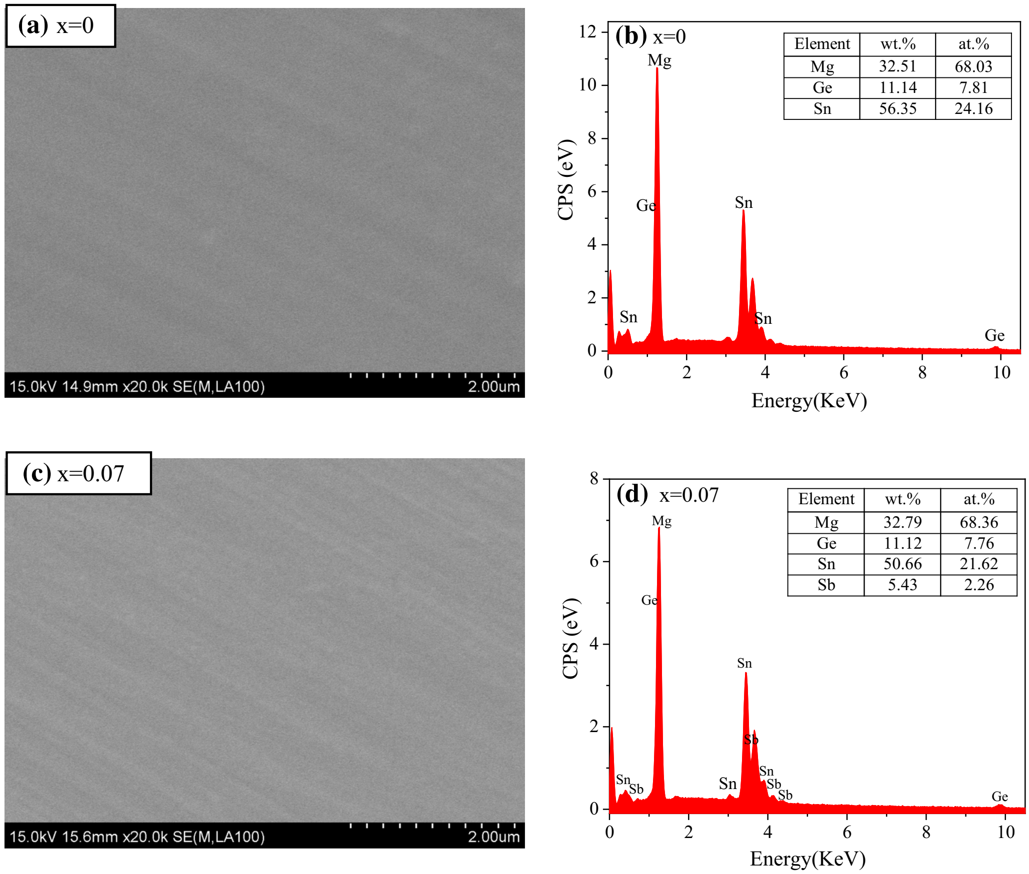

Fig. 2. Typical SEM images and EDS results for $Mg_2Ge_{0.25}Sn_{0.75}$ (a, b) and $Mg_2Ge_{0.25}Sn_{0.68}Sb_{0.07}$ (c, d) after SPS.

Table I. Electronic transport properties of $Mg_2Ge_{0.25}Sn_{0.75-x}Sb_x$ at room temperature

Specimen	Hall coefficient (cm^3 C^{-1})	Mobility (cm^2 V^{-1} s^{-1})	Carrier concentration (cm^{-3})
X = 0	−1.6	6.33	1.96×10^{18}
X = 0.03	-7.6×10^{-2}	22.29	0.82×10^{20}
X = 0.05	-6.2×10^{-2}	14.64	1.01×10^{20}
X = 0.07	-3.7×10^{-2}	13.52	1.69×10^{20}
X = 0.10	-3.4×10^{-2}	13.36	2.01×10^{20}
X = 0.15	-3.1×10^{-2}	12.89	3.86×10^{20}

phase was found, which was in good agreement with the results from XRD. The composition of the two alloys obtained by quantitative EDS analysis is listed in Fig. 2b and d, from which we can calculate the mole percent for each element. The calculated molecular formulas are $Mg_{2.11}Ge_{0.24}Sn_{0.75}$ and $Mg_{2.11}Ge_{0.24}Sn_{0.67}Sb_{0.07}$ for the two samples, respectively. The results show that the mole percents are close to the designed nominal composition both for undoped and doped alloys, except that the Mg content is slightly higher than the stoichiometry.

Thermoelectric Properties

The electronic transport properties of $Mg_2Ge_{0.25}Sn_{0.75-x}Sb_x$ at room temperature are summarized in Table I. The undoped and Sb-doped $Mg_2Ge_{0.25}Sn_{0.75}$ specimens showed n-type conduction, which means that the majority of carriers were electrons. The Hall carrier concentration n was calculated via $n = 1/Re$, where R is the Hall coefficient and e is the electric charge. The carrier concentration increased from 1.96×10^{18} cm^{-3} to 3.86×10^{20} cm^{-3} with Sb content. However, carrier mobility increased from 6.33 cm^2 V^{-1} s^{-1} to 22.29 cm^2 V^{-1} s^{-1} with Sb doping content x = 0.03, and then decreased from 22.29 cm^2 V^{-1} s^{-1} to 12.89 cm^2 V^{-1} s^{-1} with Sb doping content x increasing from 0.03 to 0.15, which is a typical behavior of semiconductors and is caused by ionized impurity scattering. At the same time, the carrier concentration increased from 1.96×10^{18} cm^{-3} to 3.86×10^{20}

cm^{-3} with Sb doping content x increasing from 0.03 to 0.15, as shown in Table I, resulting in the marked increase in electrical resistivity.

The temperature dependence of electrical resistivity and Seebeck coefficient for the $Mg_2Ge_{0.25}Sn_{0.75-x}Sb_x$ (x = 0, 0.03, 0.05, 0.07, 0.10 and 0.15) alloys is plotted in Fig. 3. As shown in Fig. 3a, the electrical resistivity increased with rising temperature, displaying a characteristic metal-like behavior, similar to that of pure $Mg_2Ge_{0.25}Sn_{0.75}$ reported previously.[21] The electrical resistivity of $Mg_2Ge_{0.25}Sn_{0.75}$ in the undoped sample is quite high, from 202 $\mu\Omega$ m at 300 K to 37 $\mu\Omega$ m at 773 K. The electrical resistivity of the Sb-doped $Mg_2Ge_{0.25}Sn_{0.75-x}Sb_x$ sample is significantly lower than that of the undoped sample and increases as the Sb content increases. For example, the electrical resistivity increases from 3.66 $\mu\Omega$ m to 9.83 $\mu\Omega$ m for the samples with Sb content increasing from x = 0.03 to x = 0.15 at 300 K. Similarly, the electrical resistivity increases from 8.48 $\mu\Omega$ m to 11.6 $\mu\Omega$ m at 773 K for the samples with Sb content increasing from x = 0.03 to x = 0.15. This may be ascribed to the reduced carrier mobility with the increasing amount of Sb substitution for Sn atoms. All samples doped with Sb show a single phase, with higher carrier concentration than undoped $Mg_2Ge_{0.25}Sn_{0.75}$, as it can provide more free electrons, but the lattice distortion caused by the Sb dopant increases with increased Sb doping content; too many lattice distortions will reduce the carrier mobility. From the above, the electrical resistivity increased throughout the temperature range with Sb doping content, but the values were all lower than that of the undoped $Mg_2Ge_{0.25}Sn_{0.75}$ alloy.

Figure 3b shows the temperature dependence of the Seebeck coefficient for $Mg_2Ge_{0.25}Sn_{0.75-x}Sb_x$. The Seebeck coefficients of the samples were found to be negative over the entire temperature range (Fig. 3b), indicating that n-type carriers (electrons) dominate the thermoelectric transport in the samples, which is in good agreement with the sign of the Hall coefficients shown in Table I. The absolute Seebeck coefficient ($|S|$) of intrinsic $Mg_2Ge_{0.25}Sn_{0.75}$ was very high (320 μV K^{-1} at 300 K), but decreased dramatically with increasing temperature (85.9 μV K^{-1} at 773 K). The values of $|S|$ increased with the increase in Sb doping content and temperature. The absolute Seebeck coefficients of the Sb-doped specimens ranged from 110 μV K^{-1} to 128 μV K^{-1} at 300 K and from 177 μV K^{-1} to 181 μV K^{-1} at 773 K. According to an earlier work,[17] as lattice distortion and band convergence are introduced, ionized impurities and ion scattering may also increase. Therefore, the scattering factor is enhanced with increased Sb content, so it is favorable for improving the Seebeck coefficient. It is thus reasonable to believe that the absolute Seebeck coefficient increases with increased Sb dopant content.

The power factor (PF) defined as $PF = \frac{S^2}{\rho}$ from the Seebeck coefficient (S) and the electrical resistivity (ρ) is plotted in Fig. 4. The Sb doping reduces the resistivity significantly and reduces the absolute Seebeck coefficients to some degree, as shown in Fig. 3. However, the PF, shown in Fig. 4, can be significantly enhanced with proper Sb doping, and increases rapidly with increasing temperature. For example, the PF values varied from 1680 μW m^{-1} K^{-2} to 3280 μW m^{-1} K^{-2} at 300 K and from 2840 μW m^{-1} K^{-2} to 3700 μW m^{-1} K^{-2} at 773 K for the Sb-doped samples with x = 0.03 to 0.15, much higher than the values of 507 μW m^{-1} K^{-2} and 196 μW m^{-1} K^{-2} at the corresponding temperatures for the undoped sample (x = 0). Compared with the undoped sample, the PF of the Sb-doped specimens was improved by around 10 times at 573 K. A maximum PF value of 4010 μW m^{-1} K^{-2} was found at 573 K for the sample with x = 0.03.

The total thermal conductivities of $Mg_2Ge_xSn_{1-x}$ alloys were shown in Fig. 5a. The thermal conductivities decreased with the increase of temperature from 300 K up to 473 K, and then increased with an increase in the measurement temperature above 473 K, indicating bipolar transport properties.[23] The total thermal conductivity for the undoped sample $Mg_2Ge_{0.25}Sn_{0.75}$ in this work decreases from

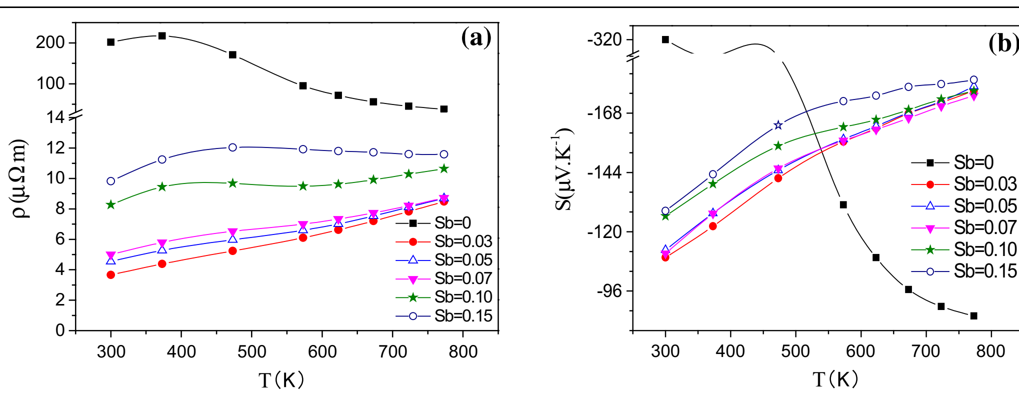

Fig. 3. Temperature dependence of (a) electrical resistivity and (b) Seebeck coefficient for the $Mg_2Ge_{0.25}Sn_{0.75-x}Sb_x$ alloys.

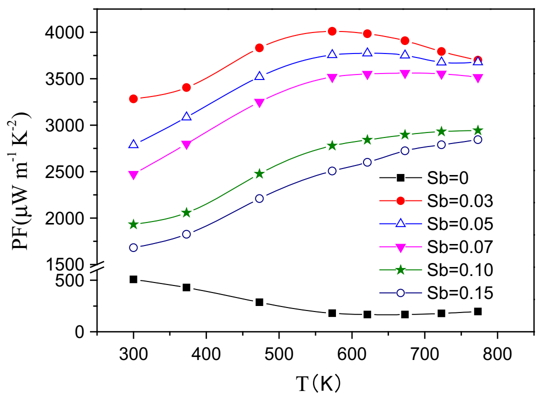

Fig. 4. Temperature dependence of power factor for the $Mg_2Ge_{0.25}Sn_{0.75-x}Sb_x$ alloys.

3.6 Wm^{-1} K^{-1} to 2.6 Wm^{-1} K^{-1} as the temperature increases from 300 K to 473 K, and gradually increases from 2.6 to 5.9 as the temperature further increases from 473 K to 773 K, which was between the previously reported thermal conductivity of pure Mg_2Ge[24] and Mg_2Sn.[23] At higher temperature, as both holes and electrons are present, this relation breaks down because bipolar diffusion takes place, and an extra term must then be added to the total thermal conductivity. The thermal conductivities of Sb-doped samples have the same variation tendency as the undoped sample and can be significantly reduced by introducing Sb into the $Mg_2Ge_{0.25}Sn_{0.75}$ lattice, as it can enhance phonon scattering caused by the substitution of Sb for Sn. The thermal conductivities for all samples were much lower than that of the pure $Mg_2Ge_{0.25}Sn_{0.75}$, and decreased with increasing Sb content. For example, thermal conductivity decreases from 3.6 Wm^{-1} K^{-1} to 1.4 Wm^{-1} K^{-1} at 300 K, 2.6 Wm^{-1} K^{-1} to 1.17 Wm^{-1} K^{-1} at 473 K, and 4.5 Wm^{-1} K^{-1} to 1.87 Wm^{-1} K^{-1} at 773 K, with Sb content x increasing from 0 to 0.15. The $Mg_2Ge_{0.25}Sn_{0.75-x}Sb_x$ samples exhibited the lowest thermal conductivity of 1.17 Wm^{-1} K^{-1} at 473 K with x = 0.10.

The total thermal conductivity (k_{tot}) can be written as a sum of the electronic (k_e) and lattice thermal conductivity (k_l). k_e is directly proportional to the electrical conductivity through the Wiedemann–Franz relation,$k_e = L\sigma T$, where L is the Lorenz number. For free electrons, $L = 2.45 \times 10^{-8}$ V^2 K^{-2}. However, for most thermoelectric materials, the real Lorenz number is lower than 2.45×10^{-8} V^2 K^{-2}, depending on the reduced Fermi energy and scattering parameter, as shown in the following.

The Seebeck coefficient (S) can be described by the Mott equation[25]:

$$S = \frac{8\pi^2 k_B^2 m^* T}{3eh^2}\left(\frac{\pi}{3n}\right)^{2/3} \quad (1)$$

where k_B is the Boltzmann constant, e is the electron charge, m^* is the effective mass of the carrier, h is the Planck constant, n is the carrier concentration and T is the absolute temperature.

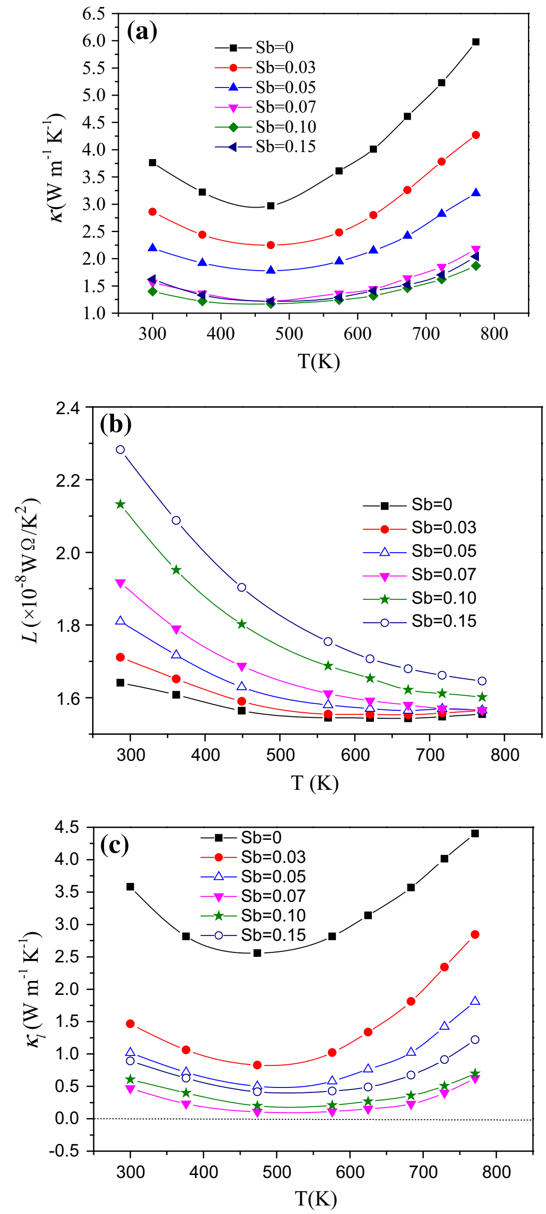

Fig. 5. Temperature dependence of (a) thermal conductivity, (b) calculated Lorenz number and (c) lattice thermal conductivity for the $Mg_2Ge_{0.25}Sn_{0.75-x}Sb_x$ alloys.

The Hall carrier concentration is related to the Fermi energy[26]:

$$n = 4\pi\left(\frac{2m^* k_B T}{h^2}\right)^{\frac{3}{2}} F_{\frac{1}{2}}(\xi) \quad (2)$$

where $F_n(\xi)$ is the Fermi integration[26];

$$F_n(\xi) = \int_0^{\infty} \frac{x^n}{1+e^{x-\xi}}\,dx \quad (3)$$

The reduced Fermi energy can be derived from both the carrier concentration and Seebeck coefficient on the basis of single-band approximation[26]:

$$S = \frac{k_B}{e}\left(\frac{(\lambda + 5/2)F_{\lambda+3/2}(\xi)}{(\lambda + 3/2)F_{\lambda+1/2}(\xi)} - \xi\right) \tag{4}$$

In the equation, k_B is the Boltzmann constant, ξ is the reduced Fermi energy and h is the Planck constant. It is clearly shown that the evaluation of ξ from the measured S is only related to scattering parameter λ while the estimation of ξ from the measured n is associated with two unknown parameters m^* and λ. So the calculation of ξ is derived from the measured S by using Eqs. 3 and 4. Here, acoustic phonon scattering has been assumed as the main carrier scattering mechanism near room temperature, i.e., $\lambda = -0.5$. The Lorenz number L is calculated by employing a single parabolic band model[26]:

$$L = \left(\frac{k_B}{e}\right)^2\left(\frac{(\lambda+7/2)F_{\lambda+5/2}(\xi)}{(\lambda+3/2)F_{\lambda+1/2}(\xi)} - \left[\frac{(\lambda+5/2)F_{\lambda+3/2}(\xi)}{(\lambda+3/2)F_{\lambda+1/2}(\xi)}\right]^2\right) \tag{5}$$

As stated above, the values of L obtained from this method are most accurate for moderate temperatures where the single-band model applies, and are plotted in Fig. 5b. The L values decrease with increasing T but increase with the Sb doping level. The lattice thermal conductivities k_l obtained by the calculated Lorenz numbers are presented in Fig. 5c. It can be seen that the k_l of Sb-doped samples decreases with the Sb doping content, which may be attributed to lattice distortion and microstructural defects arising from Sb doping. The huge decease in the k_l leads to a direct decrease in the total thermal conductivity of the $Mg_2Ge_xSn_{1-x}$ solutions. The k_l decreases with increasing T for moderate temperature, suggesting that k_l decreases due to an increase in phonon–phonon scattering with rising temperature. This phenomenon is also observed in the $Sb_xPb_{1-x}Te_{0.88}S_{0.12}$ and $Mg_2Si_{0.5}Ge_{0.5}Sb_m$ systems.[27,28]

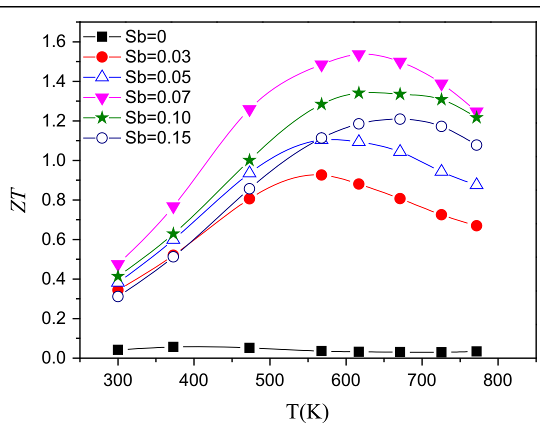

Fig. 6. Temperature dependence of ZT for the $Mg_2Ge_{0.25}Sn_{0.75-x}Sb_x$ alloys.

The figures of merit (ZT) for the studied samples, shown in Fig. 6, were calculated by the equation $ZT = S^2\sigma T/k$ from the above data. The results indicated that the values of ZT for Sb-doped samples were greatly improved and increased with increasing temperature for temperatures lower than 600 K. The ZT values for all Sb-doped samples were markedly higher than that for the undoped sample (less than 0.1). The sample of the $Mg_2Ge_{0.25}Sn_{0.75-x}Sb_x$ with $x = 0.07$ showed the highest ZT value of 1.54 at 623 K, due to its lower thermal conductivity, lower electrical resistivity and somewhat higher Seebeck coefficient, which was higher than the value of 1.4 for the Sb-doped $Mg_2Ge_{0.25}Sn_{0.75}$ alloy at 773 K,[21] and 1.4 was practically the highest ZT value reported recently in Mg_2X system.[29]

CONCLUSION

The results of the study show that $Mg_2Ge_xSn_{1-x}$ (x = 0.15, 0.20, 0.25 and 0.30) and $Mg_2Ge_{0.25}Sn_{0.75-x}Sb_x$ (x = 0, 0.03, 0.05, 0.07, 0.10 and 0.15) were able form solid solutions by high-frequency melting, annealing and spark plasma sintering. Investigation of the effects of Sb substitution on the phase constitution and thermoelectric properties of the $Mg_2Ge_{0.25}Sn_{0.75-x}Sb_x$ solution revealed that the $Mg_2Ge_xSn_{1-x}$ and $Mg_2Ge_{0.25}Sn_{0.75-x}Sb_x$ solid solutions were well formed, and no second phase was found after Sb doping. The lattice constants of $Mg_2Ge_{0.25}Sn_{0.75-x}Sb_x$ decreased gradually from 6.689 Å to 6.672 Å with increasing Sb content. The distortions and changes in carrier concentration caused by the substitution of the Sb atoms for the Sn atoms in these single phases led to electrical and thermal transport, thus enhancing the thermoelectric performance. The electrical resistivity of the solid solution decreased significantly with the substitution of Sb for Sn, and the Seebeck coefficient for all samples was reduced slightly by Sb doping, but thermal conductivity was obviously reduced. As a result, the figures of merit of the samples were drastically improved. With the appropriate Sb dopant, the highest figure of merit ZT value of 1.54 was obtained in the sample $Mg_2Ge_{0.25}Sn_{0.68}Sb_{0.07}$ at 623 K. The doping of Sb and point defects such as interstitial Mg and Ge/Sn vacancies caused by the over-stoichiometric Mg have a positive effect on the electron concentration and thermoelectric properties of n-type Mg_2Sn_x-based compounds.

ACKNOWLEDGMENTS

The work was supported by the National Natural Science Foundation of China (Nos: 51101103, 51171117 and 51571144), and Shenzhen Science and Technology Research Grant (Nos. JCYJ20150827155136104, JCYJ20150324141711684 and JCYJ20150069). The authors would like to thank Mr. Haizhao Yu and Jun Pei for their help with the experiment.

REFERENCES

1. J. He, Y. Liu, and R. Funahashi, *J. Mater. Res.* 26, 1762 (2011).
2. S.R. Sankar, D.P. Wong, C.S. Chi, W.L. Chien, J.S. Hwang, F.C. Chou, L.C. Chen, and K.H. Chen, *CrystEngComm* 17, 3440 (2015).
3. T.C. Harman, P.J. Taylor, M.P. Walsh, and B.E. LaForge, *Science* 297, 2229 (2002).
4. B. Poudel, Q. Hao, Y. Ma, Y. Lan, A. Minnich, B. Yu, X. Yan, D. Wang, A. Muto, D. Vashaee, X. Chen, J. Liu, M.S. Dresselhaus, G. Chen, and Z. Ren, *Science* 320, 634 (2008).
5. W.T. Liu, X.F. Tang, H. Li, J. Sharp, X.Y. Zhou, and C. Uher, *Chem. Mat.* 23, 5256 (2011).
6. S.W. You and I.H. Kim, *J. Korean Phys. Soc.* 64, 690 (2014).
7. S. Nakamura, Y. Mori, and K.I. Takarabe, *J. Electron. Mater.* 43, 2174 (2014).
8. K. Kambe and H. Udono, *J. Electron. Mater.* 43, 2212 (2014).
9. X.K. Hu, D. Mayson, and M.R. Barnett, *J. Alloys Compd.* 589, 485 (2014).
10. H. Gao, T. Zhu, X. Zhao, and Y. Deng, *Dalton Trans.* 43, 14072 (2014).
11. J. de Boor, C. Compere, T. Dasgupta, C. Stiewe, H. Kolb, A. Schmitz, and E. Mueller, *J. Mater. Sci.* 49, 3196 (2014).
12. S.W. You, D.K. Shin, and I.H. Kim, *J. Korean Phys. Soc.* 64, 1346 (2014).
13. M. Akasaka, T. Iida, A. Matsumoto, K. Yamanaka, Y. Takanashi, T. Imai, and N. Hamada, *J. Appl. Phys.* 104, 013703 (2008).
14. H.L. Gao, X.X. Liu, T.J. Zhu, S.H. Yang, and X.B. Zhao, *J. Electron. Mater.* 40, 830 (2011).
15. M.A.B. Bashir, S.M. Said, M.F.M. Sabri, D.A. Shnawah, and M.H. Elsheikh, *Renew. Sust. Energy Rev.* 37, 569 (2014).
16. W. Liu, X.J. Tan, K. Yin, H.J. Liu, X.F. Tang, J. Shi, Q.J. Zhang, and C. Uher, *Phys. Rev. Lett.* 108, 166601 (2012).
17. X. Zhang, H.L. Liu, S.H. Li, F.P. Zhang, Q.M. Lu, and J.X. Zhang, *Mater. Lett.* 123, 31 (2014).
18. X.K. Hu, M.R. Barnett, and A. Yamamoto, *J. Alloys Compd.* 649, 1060 (2015).
19. S.W. You, D.K. Shin, and I.H. Kim, *J. Korean Phys. Soc.* 65, 691 (2014).
20. P. Villars, A. Prince, and H. Okamoto, *Handbook of Ternary Alloy Phase Diagrams* (New York: ASM International, 1995), pp. 236–237.
21. W.S. Liu, H.S. Kim, S. Chen, Q. Jie, B. Lv, M. Yao, Z. Ren, C.P. Opeil, S. Wilson, C.W. Chu, and Z. Ren, *Proc. Natl. Acad. Sci. U.S.A.* 112, 3269 (2015).
22. S.J. Su, B.W. Cheng, C.L. Xue, D.L. Zhang, G.Z. Zhang, and Q.M. Wang, *Acta Phys. Sin.* 61, 176104 (2012).
23. S.M. Choi, T.H. An, W.S. Seo, C. Park, I.H. Kim, and S.U. Kim, *J. Electron. Mater.* 41, 1071 (2012).
24. H.L. Gao, T.J. Zhu, X.B. Zhao, and Y. Deng, *Intermetallics* 56, 33 (2015).
25. S. Sharma and S.K. Pandey, *Comp. Mater. Sci.* 85, 340 (2014).
26. C.M. Bhandari and D.M. Rowe, *Thermal Conduction in Semiconductors* (New York: Wiley, 1988), pp. 115–119.
27. J.Q. Li, X.X. Li, F.S. Liu, W.Q. Ao, and H.T. Li, *J. Electron. Mater.* 42, 366 (2013).
28. S.W. You, D.K. Shin, S.C. Ur, and I.H. Kim, *J. Electron. Mater.* 44, 1504 (2015).
29. G.S. Polymeris, N. Vlachos, A.U. Khan, E. Hatzikraniotis, C.B. Lioutas, A. Delimitis, E. Pavlidou, K.M. Paraskevopoulos, and T. Kyratsi, *Acta Mater.* 83, 285 (2015).